Study of heat transfer characteristics in PCFG fabrication technology using heat method

Yuefeng Qi (齐跃峰)*, Hanping Qiao (乔汉平), and Weihong Bi (毕卫红)

Institute of Information Science and Engineering, Yanshan University, Qinhuangdao 066004, China

**Corresponding author: yfqi@ysu.edu.cn*

Received August 17, 2010; accepted November 26, 2010; posted online January 28, 2011

The fiber gratings fabrication technology with the heating method in a photonic crystal fiber (PCF) based on structural change is examined. The principle of photonic crystal fiber gratings (PCFGs) is analyzed in theory. The heat transfer theory and finite element method are used to examine the thermal field distribution in the fiber and the influence of the air hole structure in the cladding, and the parameters of the laser beam in the process of grating fabrication are discussed. The results show that gratings can be formed by the periodic collapse of air holes in the cladding of PCFs. Under double-point heating condition, the energy is uniformly distributed in the radial direction and is approximate to Gaussian distribution in the axial direction. With the same size of the luminous spot, as the layers and radius of the air holes increase, the laser power needed to make the air holes collapse decreases. With the same laser power, as the luminous spot radius increases, the needed heating time increases. Moreover, the relationship between the laser power needed and the air filling rate is obtained as the number of layers of the air holes changes from 1 to 7. This kind of PCFG can overcome the long-term thermal instability of conventional gratings in substance and thus has great potential applications in the related field of optical fiber sensors.

OCIS codes: 060.3735, 060.4005.

doi: 10.3788/COL201109.020605.

Photonic crystal fibers (PCFs) are all-silica fibers in which an array of air holes is distributed in the cladding and extends along the length of the fiber. They have special optical characteristics so that they have attracted much attention. In recent years, the fabrication technology and theoretical study of photonic crystal fiber gratings (PCFGs) have become a new research focus. Compared with the conventional fiber gratings on the single mode fiber, PCFGs have superior performance[1]. They have great potential applications in optical fiber communication, optical fiber sensors, and many other fields[2,3].

At present, the ultraviolet (UV) exposure method is commonly used for the fabrication of fiber gratings. With phase masks, the gratings are written in fiber-doped Ge/B or loaded hydrogen. The advantages of this technology are its maturity and ease of use. However, it is limited by the fact that the grating performance deteriorates over time, which means that long-term stability is difficult to maintain[4]. In addition, the gratings decay or are even erased completely under a high-temperature environment[5], so the thermal stability is also undesirable. These disadvantages greatly restrict the technology's applications in some fields.

The structural change method used in the fabrication of PCFGs was first proposed by Yinian *et al*. of Nanyang Technological University in Singapore in 2003[6]. Using total internal reflection PCF in pure silica, they employed CO_2 laser as heat source to make the air holes collapse according to the preset distance. The collapse of the air holes can change the refractive index in the cladding, so the long period gratings in PCF (LPG-PCF) can be formed. This kind of grating fabrication technology needs neither dope B/Ge nor load hydrogen in the fiber; it merely relies on the deformation of PCFs to fabricate gratings. An obvious deformation can be induced by prolonging the heating time, so the coupling between the fundamental core mode and a set of forward-propagation cladding modes can be enhanced with an increase in modulation of the refractive index along the axis. This kind of LPG-PCF based on structural change is more strain sensitive than that with no structural change[7].

In this letter, the principle involved in the heating method of LPG-PCF based on structural change is investigated, and the distribution of the effective refractive index is computed. With CO_2 laser as the heating source, the distribution model of the thermal field is established, and the heat transfer characteristics in the fiber are analyzed. The effects of air hole structure, laser power, and luminous spot radius on the grating fabrication process are discussed. As a result, the mathematical relationship between the laser power and the air filling rate is obtained.

Using the multipolar method[8,9], the effective refractive index of the cladding of PCF with collapsed air holes is examined. The data can be fitted with a five-order function, and the distribution expression of the effective index in the collapsed segment of the fiber along the axis direction can be obtained[10]:

$$f(z) = \sum_{k=0}^{5} a_k \mathrm{e}^{kz}, \quad -\frac{w}{2} \le z \le \frac{w}{2}, \tag{1}$$

where w is the width of collapse, and a_k is the expansion coefficient which depends on matrix A:

$$A = \begin{bmatrix} 1.138 \times 10^7, -5.581 \times 10^7 \\ 1.636 \times 10^8, -3.187 \times 10^8 \\ 4.331 \times 10^8, -4.189 \times 10^8 \end{bmatrix}.$$

After PCF is heated by the heating method, the deformation of the collapsed PCF in the longitudinal direction is shown in Fig. 1.

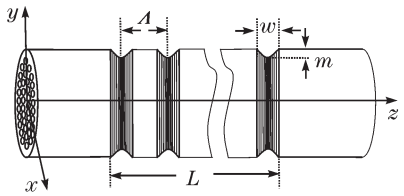

Fig. 1. Collapsed PCF.

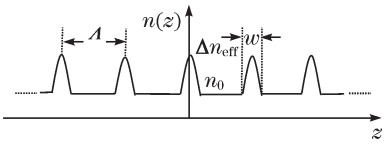

Fig. 2. Distribution of the refractive index in LPG-PCF.

In Fig. 1, Λ is the collapse period which is also the grating period, the collapse width w is determined by the luminous spot radius, and m is the collapse depth which depends on the laser power and heating time. In the condition of heating, the profile of the collapsed PCF is similar to a periodic function according to the result of the experiment and the above investigation as shown in Eq. (1). The distribution model of the refractive index is shown in Fig. 2. The refractive index is assumed to be distributed uniformly in the radial direction.

In Fig. 2, n_0 is the effective refractive index of PCF which does not collapse, and Δn_{eff} is the maximum of the effective refractive index in the collapsed segment which is the modulation amplitude of the refractive index. $n\,(z)$ can be expressed as

$$n(z) = \begin{cases} n_0 + f(z) & k\Lambda - w/2 \le z \le k\Lambda + w/2 \\ n_0 & k\Lambda - w/2 > z, z > k\Lambda + w/2 \end{cases}, \quad (2)$$

where k is an integer. Substituting Eq. (1) into Eq. (2) and expanding the Fourier series, the expression with the top five orders can be obtained:

$$n(z) = n_0 + \sum_{k=0}^{5} b_k \cos\left(k\frac{2\pi}{\Lambda}z\right), \quad (3)$$

where b_k is the Fourier expansion coefficient depending on the matrix B:

$$B = \begin{bmatrix} 1.435000000, & -0.00882 \\ -0.0002008, & -0.1478305 \\ -0.0001246, & -0.0004898 \end{bmatrix}.$$

Equation (3) has given the refractive index distribution in LPG-PCF. Then using the coupled mode theory, the resonant wavelength, reflectivity, and other grating performance parameters can be obtained.

The distribution of the thermal field in PCF during the process of grating fabrication with heating from CO_2 laser is very important. In this letter, using the heat transfer theory and the finite element method[11], the distribution of the thermal field in PCF under different heating conditions is analyzed.

The PCF used in this study has a core surrounded by seven layers of air holes which are of hexagonal distribution. The outer diameter is 125 μm, the diameter of the air holes is 2.2 μm, and the spacing between holes is 5 μm. The double-point heating pattern is used. The mesh of the finite element simulation is shown in Fig. 3, and the triangles generated in the surface and the tetrahedrons appear in three-dimensional (3D) space. Neumann boundary conditions are adopted. To reduce the calculation work, a 2-mm-long fiber is used in the analysis. The parameters of the PCF material are listed in Table 1.

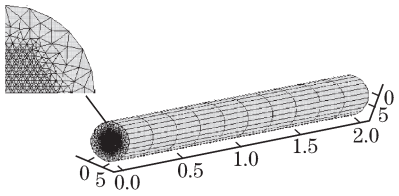

Fig. 3. Schematic mesh picture of the cross section and air holes of PCF.

Table 1. Material Property

Material Property	SiO_2	Air
Density ρ (kg·m^{-3})	2200	0.93
Specific Heat c_{p} (J·kg^{-1}·K^{-1})	1345	1010
Thermal Conductivity k (W·m^{-1}·K^{-1})	2.68	0.032
Melting Point (K)	1976	

According to the Fourier law of heat transfer and the energy conservation law[12], the 3D mathematical model of heat transfer is shown as

$$\frac{\partial T}{\partial t} - \frac{k}{\rho c_{\text{p}}}\nabla^2 T = 0, \quad (4)$$

where T is the temperature, t is the time, and k, ρ, and c_{p} are the thermal conductivity, density, and specific heat, respectively.

Using the cylindrical coordinate system, the heat transfer equation can be obtained as

$$\rho C_{\text{p}}\frac{\partial T}{\partial t} = \frac{1}{r}\frac{\partial}{\partial r}\left(kr\frac{\partial T}{\partial r}\right) + \frac{1}{r^2}\frac{\partial}{\partial \phi}\left(k\frac{\partial T}{\partial \phi}\right) + \frac{\partial}{\partial z}\left(\frac{\partial T}{\partial z}\right). \quad (5)$$

The boundary conditions are

$$\begin{cases} -k\dfrac{\partial T}{\partial r} = q(r,\phi,z), & r = R,\ 0 \le z \le 200 \\ \dfrac{\partial T}{\partial r} = 0, & r = R,\ 200 < z \le \infty \\ \dfrac{\partial T}{\partial r} = 0, & r = 0 \end{cases}, \quad (6)$$

where z refers to the axial coordinate in the fiber, R is the radius of the fiber, and q is the heat flux.

The initial conditions are

$$T = T_0 = 298\ \text{K}, \quad t = 0, \quad 0 \le r \le R. \quad (7)$$

The differential equation for the temperature field is obtained by Eq. (5) as

$$\Omega[T(x,y,z,t)] = k\left(\frac{\partial^2 T}{\partial x^2}+\frac{\partial^2 T}{\partial y^2}+\frac{\partial^2 T}{\partial z^2}\right)+Q-\rho C_{\mathrm{p}}\frac{\partial T}{\partial t}=0. \quad (8)$$

Substituting the trial function $\widetilde{T}$ and the Gaussian formulas into Eq. (5) and utilizing the boundary relationship of region Ω, the following equation is obtained:

$$\frac{\partial J^{\Omega}}{\partial T_j}=\iiint_{\Omega}\left[k\left(\frac{\partial W_j}{\partial x}\frac{\partial \widetilde{T}}{\partial x}+\frac{\partial W_j}{\partial y}\frac{\partial \widetilde{T}}{\partial y}+\frac{\partial W_j}{\partial z}\frac{\partial \widetilde{T}}{\partial z}\right)\right]\mathrm{d}x\mathrm{d}y\mathrm{d}z-\iiint_{\Omega}\left(QW_j+\rho C_{\mathrm{p}}W_j\frac{\partial \widetilde{T}}{\partial t}\right)\mathrm{d}x\mathrm{d}y\mathrm{d}z-\oiint_{\Sigma}kW_j\frac{\partial \widetilde{T}}{\partial \vec{n}}\mathrm{d}\vec{s}=0 \quad (j=1,2,\cdots,n), \quad (9)$$

where W_j is the weight function, $\vec{n}$ is the normal vector of the boundary, Ω is the domain of the temperature field, and Q is the quantity of heat that an object receives per one unit of time. This is the fundamental equation for calculating the 3D temperature field using the finite element method.

If the region Ω is divided into E units and n nodes, then the temperature field can be discretized as the undetermined temperature in n nodes, namely, T_1, T_2, $\cdots$, T_n. Then the calculus of variations can be carried out, and the following equation can be isolated from Eq. (9):

$$\frac{\partial J^{e}}{\partial T_j}=\iiint_{\Omega}\left[k\left(\frac{\partial W_j}{\partial x}\frac{\partial \widetilde{T}}{\partial x}+\frac{\partial W_j}{\partial y}\frac{\partial \widetilde{T}}{\partial y}+\frac{\partial W_j}{\partial z}\frac{\partial \widetilde{T}}{\partial z}\right)-QW_j+\rho C_{\mathrm{p}}W_j\frac{\partial \widetilde{T}}{\partial t}\right]\mathrm{d}x\mathrm{d}y\mathrm{d}z-\oiint_{\Sigma_e}kW_j\frac{\partial \widetilde{T}}{\partial \vec{n}}\mathrm{d}\vec{s} \quad (j=i,l,m,p), \quad (10)$$

where i, l, m, and p are the node numbers of the units' local, and they are also the four vertices of the tetrahedron with the finite element method.

Substituting Eq. (10) into Eq. (9), all the algebraic equations can be synthesized:

$$\frac{\partial J^{\Omega}}{\partial T_j}=\sum_{e=1}^{E}\frac{\partial J^{e}}{\partial T_j}=0 \quad (j=1,2,\cdots,n). \quad (11)$$

With n algebraic equations, the temperature in n nodes can be obtained. After organization, the matrix equation is obtained as

$$[C]\left\{\dot{T}\right\}+[K]\{T\}=\{Q\}, \quad (12)$$

where $[K]$ is the transfer matrix including the heat transfer coefficients and convection coefficients, $[C]$ is the specific heat matrix, $\{T\}$ is the node temperature vector, $\{\dot{T}\}$ is the time derivative of temperature, and $\{Q\}$ is the temperature loading of the internal heat source.

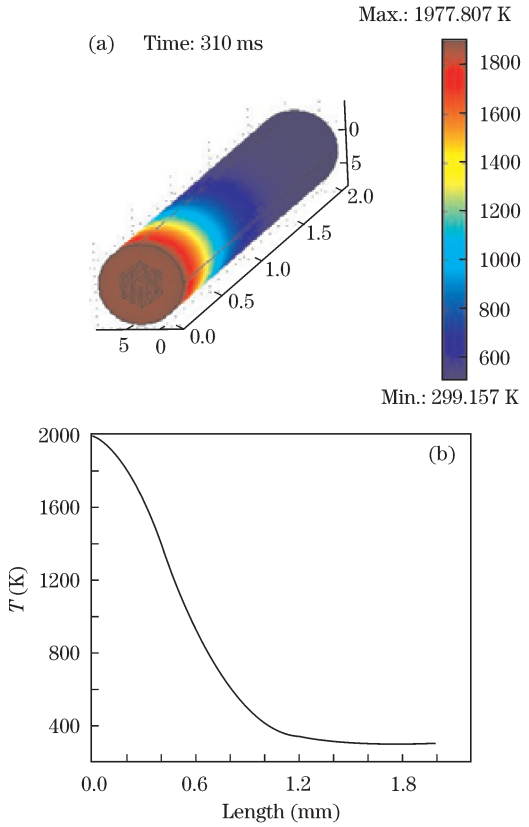

Fig. 4. (a) Simulated heat transfer results for PCF; (b) temperature profile as a function of length for PCF.

With the above methods, the PCFG with a structure of seven layers of air holes is simulated for the heating process, and the temperature field distributions in the vertical and radial directions of the fiber are analyzed. The laser power is 1.6 W, the luminous spot radius is 100 μm, the heating time is 310 ms, and the fiber length is 2 mm. On the fiber surface, the temperature field distribution along the z axis is shown in Fig. 4.

From Fig. 4, the temperature distribution along the z direction is known to be Gaussian distribution, which coincides with the energy distribution. In addition, the heat energy is mainly concentrated in the range less than 0.6 mm. The temperature at the center of the heat source is 1977 K, achieving the melting point of SiO_2. The temperature is 1800 K at 0.2 mm of the fiber, and the temperature is close to the initial temperature of fiber (298 K) at 2 mm of the fiber. Thus, using the CO_2 laser heating method, SiO_2 can achieve the melting point in the range of tens to hundreds of micrometers, and air hole collapse can be realized. This results in the formation of long period gratings. Further, Fig. 3 shows that the temperature distribution in the cross section of the fiber is not affected when the 2-mm-long fiber is selected. The simulation results are not influenced as well.

The temperature distribution in the radial direction is shown in Fig. 5. From Fig. 5(a), the isotherms are distributed along the radial direction, and the temperatures are almost equal when there is the same distance from the fiber core. However, the temperature changes in the positions where there are air holes. The temperature difference between the internal and external cross

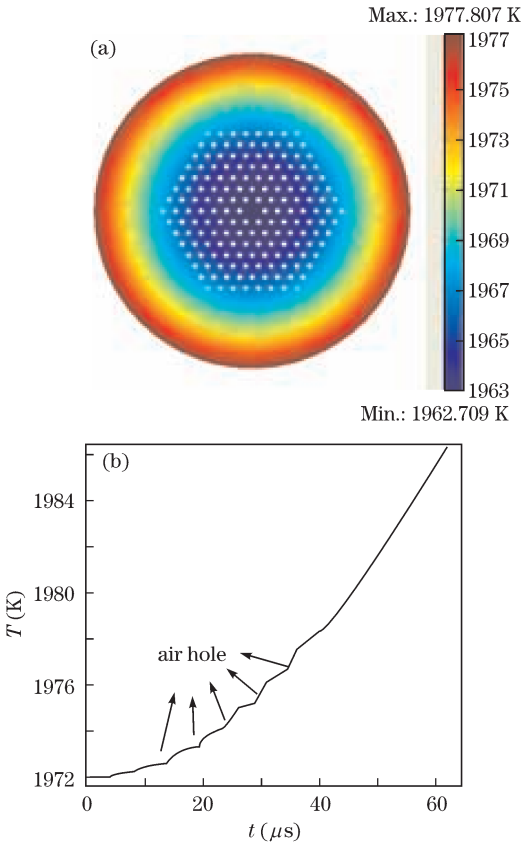

Fig. 5. (a) Temperature distribution of the cross section of PCF; (b) radial temperature curve at 310 ms.

sections of the fiber is only 14 K (less than 1%). It reaches the melting point of SiO_2 and accords with the heating conditions.

The curve of the temperature distribution (shown in Fig. 5(b)) when the collapse condition in the radial direction is reached. From this figure, the air holes are shown to affect the heating process. The temperature distribution in the air holes is almost linear, and there exists a large temperature gradient. Comparing the temperature gradient in the air holes with that in SiO_2, the latter is very small. This is because the thermal conductivity of air is far less than that of SiO_2, and air obstructs the heat transfer.

To analyze the effect of laser beam parameters, the heating process is simulated with different laser powers and luminous spot radii, respectively. The results are shown in Fig. 6.

Figure 6(a) shows the relationship between the laser power and the required heating time when the luminous spot radius is 100 μm. From this figure, with the same laser spot radius, the heating time leading to PCF collapse decreases as the laser power increases. When the power of the laser is 2 W, the heating time is only 182 ms. When the power of the laser is 1 W, the heating time becomes 646 ms, which is much larger than that at 2 W. Considering the response time and stability of the laser output in the practical operation of PCFG carving, the most appropriate output power is 1.6 W.

Figure 6(b) shows the relationship between the luminous spot radius and the required heating time when the laser power is 1.6 W. At the same laser power, as the

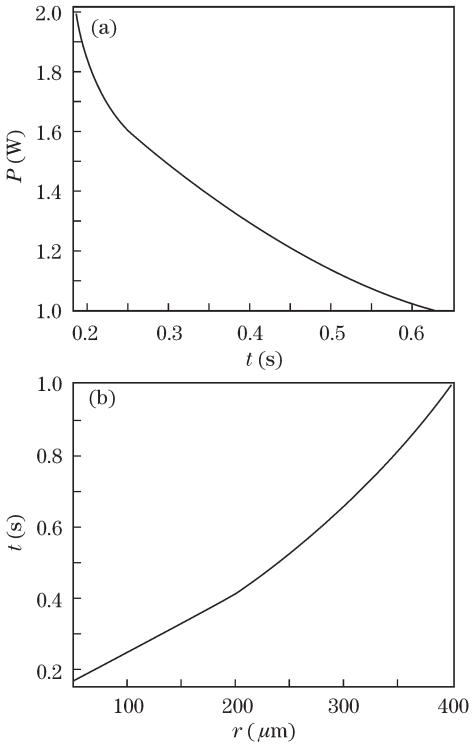

Fig. 6. (a) Curve of the collapse time t under different heating powers P with spot radius $r = 100$ μm; (b) curve of the collapse time t under different spot radii r with laser power $P = 1.6$ W.

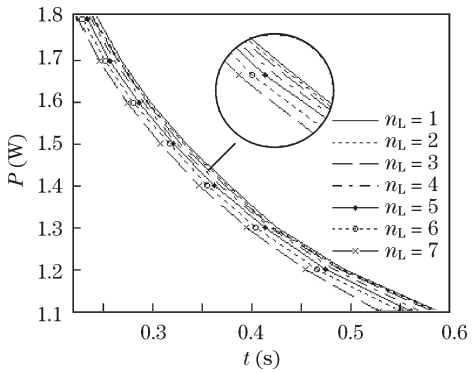

Fig. 7. Variation in heating power under different numbers of air hole layers n_L.

luminous spot radius increases, the heating time increases. This is because the energy distribution is mainly determined by the laser spot radius. When the laser power is not changed, as the spot radius enlarges, the heat flux of the fiber surface decreases.

To analyze the effect of the air hole structure on the heating process, PCF models with different layers and diameters of air holes are built and simulated. The results are shown in Figs. 7 and 8, respectively.

If the numbers of air hole layers are not the same, the velocities of heat transfer in the radial direction of PCF will be very different. At the same spot radius and air hole diameter (1.6 μm), the PCF layers increase from 1 to 7, when the PCF attains the collapse temperature. The simulation results of the relationship between the laser power and the heating time are shown in Fig. 7. In

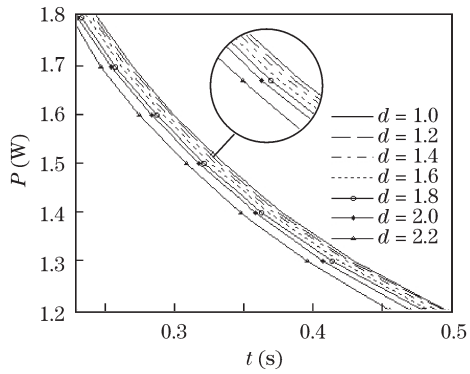

Fig. 8. Variation in heating power with different air hole radii d at the same fiber radius R.

this figure, when there is a change in the course of air hole layers from 1 to 7, the heating time decreases as the laser power increases, and their variation regularities look the same. The difference is that under the same heating power, the more are the layers, the less time is required to achieve the same temperature.

With the same number of air hole layers and fiber radius R, when the PCF achieves the collapse temperature, the relationship between the heating power and the air hole radius is shown in Fig. 8. From the figure, for a PCF with a certain air hole radius, the heating time for the collapse temperature increases as the heating power decreases, and the downtrend of all curves is obvious. With the same laser power, as the air hole radius increases, the heating time for collapse temperature reduces. A further examination also shows that at the same air hole radius, as the number of air hole layers increases, the heating energy decreases. When the number of air hole layers increases from 1 to 7, the variation in heating energy is around 0.4 W.

In conclusion, we deal with the fabrication technology of PCFG based on its structural change with the heating method. A theoretical analysis of this fabrication technology is presented, and the temperature field distribution is computed. In the grating fabrication process, the effects of laser beam parameters and fiber structure on PCFG are discussed. An in-depth investigation has been done on the law of temperature field distribution in PCF under heating condition. Using the results, when the PCF structural parameters and the desired PCFG structure are known, the required laser spot size, laser power, and time parameters can be calculated. Overall, we have provided a theoretical basis for the fabrication of PCFG with the heating method and proposed a theoretical guidance for its further development.

This work was supported by the National Basic Research Program of China (No. 2010CB327801), the Natural Science Foundation of Hebei Province, China (No. F2010001286), and the Applied Basic Research Projects of Hebei Province, China (No. 10963526D).

References

1. B. J. Eggleton, P. S. Westbrook, R. S. Windeler, S. Spälter, and T. A. Strasser, Opt. Lett. **24,** 1460 (1999).
2. J. E. Sharping, M. Fiorentino, P. Kumar, and R. S. Windeler, IEEE Photon. Technol. Lett. **14,** 77 (2002).
3. A. I. Siahlo, L. K. Oxenlwe, K. S. Berg, A. T. Clausen, P. A. Andersen, C. Peucheret, A. Tersigni, P. Jeppesen, K. P. Hansen, and J. R. Folkenberg, IEEE Photon. Technol. Lett. **15,** 1147 (2003).
4. B.-O. Guan, H.-Y. Tam, X.-M. Tao, and X.-Y. Tao, IEEE Photon. Technol. Lett. **12,** 1349 (2000).
5. L. Dong and W. F. Liu, Appl. Opt. **36,** 8222 (1997).
6. Y. Zhu, P. Shum, H.-J. Chong, M. K. Rao, and C. Lu, Opt. Express **11,** 1900 (2003).
7. Z. Zhou, Z. Wang, P. Xie, and T. Jing, Laser Optoelectron. Prog. (in Chinese) **42,** (8) 41 (2005).
8. T. P. White, B. T. Kuhlmey, R. C. McPhedran, D. Maystre, G. Renversez, C. Martijn de Sterke, and L. C. Botten, J. Opt. Soc. Am. B **19,** 2322 (2002).
9. B. T. Kuhlmey, T. P. White, G. Renversez, D. Maystre, L. C. Botten, C. Martijn de Sterke, and R. C. McPhedran, J. Opt. Soc. Am. B **19,** 2331 (2002).
10. Y. Qi, W. Bi, Y. Liu, and Y. Wang, Acta Opt. Sin. (in Chinese) **30,** 1178 (2010).
11. G. Fu, W. Bi, and W. Jin, Chinese J. Lasers (in Chinese) **36,** 2966 (2009).
12. A. Singh, I. V. Singh, and R. Prakash, Int. J. Heat Mass Transfer **50,** 1212 (2007).